HOSTED BY

ELSEVIER

Available online at www.sciencedirect.com

ScienceDirect

Progress in Natural Science: Materials International 25 (2015) 342–352

Progress in Natural Science Materials International

www.elsevier.com/locate/pnsmi
www.sciencedirect.com

Original Research

Low-temperature SCR activity and SO_2 deactivation mechanism of Ce-modified V_2O_5–WO_3/TiO_2 catalyst

Ziran Ma[a,b], Xiaodong Wu[a,*], Ya Feng[a], Zhichun Si[c], Duan Weng[a,c,**], Lei Shi[d]

[a]The Key Laboratory of Advanced Materials of Ministry of Education, School of Materials Science and Engineering, Tsinghua University, Beijing 100084, China
[b]National Institute of Clean-and-Low-Carbon Energy (NICE), Beijing 102209, China
[c]Advanced Materials Institute, Graduate School at Shenzhen, Tsinghua University, Shenzhen 518055, China
[d]Redbud Innovation Institute, Longyan, Fujian 364000, China

Received 6 February 2015; accepted 4 May 2015
Available online 30 August 2015

Abstract

The promotion effect of ceria modification on the low-temperature activity of V_2O_5-WO_3/TiO_2 catalyst was evaluated for the selective catalytic reduction of NO with NH_3 (NH_3-SCR). The catalytic activity of 1 wt% V_2O_5-WO_3/TiO_2 was significantly enhanced by the addition of 8 wt% ceria, which exhibited a NO_x conversion above 80% in a broad temperature range 190–450 °C. This performance was comparable with 3 wt% V_2O_5-WO_3/TiO_2, indicating that the addition of ceria contributed to reducing the usage of toxic vanadia in developing low-temperature SCR catalysts. Moreover, V1CeWTi exhibited approximately 10% decrease in NO_x conversion in the presence of 60 ppm SO_2. The characterization results indicated that active components of V, W and Ce were well dispersed on TiO_2 support. The synergetic interaction between Ce and V species by forming V–O–Ce bridges enhanced the reducibility of VCeWTi catalyst and thus improved the low-temperature activity. The sulfur poisoning mechanism was also presented on a basis of the designed TPDC (temperature-programmed decomposition) and TPSR (temperature-programmed surface reaction) experiments. The deposition of $(NH_4)_2SO_4$ on V1CeWTi catalyst was much smaller compared with that on V1Ti. On the other hand, the oxidation of SO_2 to SO_3 was significantly promoted on the CeO_2-modified catalyst, accompanied by the formation of cerium sulfates. Therefore, the deactivation of this catalyst was mainly attributed to the vanishing of the V–Ce interaction and the sulfation of active ceria.

Keywords: V_2O_5-WO_3/TiO_2; Ceria; NH_3-SCR; Low-temperature activity; SO_2 poisoning

1. Introduction

The selective catalytic reduction of NO with NH_3 (NH_3-SCR) in the presence of excess oxygen has been proved the most effective technique applied for the removal of NO_x from stationary sources and diesel exhausts [1–5]. V_2O_5-WO_3/TiO_2 (VWTi) catalyst has been the most widespread catalyst in industrial application for decades, which exhibits high efficiency at 300–450 °C [1,2]. However, there are some drawbacks remaining for this type of catalyst, such as the thermal instability of vanadia and anatase support and the lowered N_2 selectivity at high temperatures (450–500 °C) due to the high NH_3 oxidation activity [1,2,5].

Moreover, the activity of VWTi catalysts is evidently limited at temperatures lower than 300 °C, which degrades the systematic performance of the industrial deNO_x installation [2,4]. Reheating the low-temperature exhaust gas by heat exchanger has also been successfully applied in deNO_x installation with some specific layouts [4], which to some extent ensures the efficiency of denitration. However, this

*Corresponding author. Tel.: +86 10 62792375.
**Corresponding author at: The Key Laboratory of Advanced Materials of Ministry of Education, School of Materials Science and Engineering, Tsinghua University, Beijing 100084, China. Tel.: +86 10 62785986.
E-mail addresses: wuxiaodong@tsinghua.edu.cn (X. Wu), duanweng@tsinghua.edu.cn (D. Weng).
Peer review under responsibility of Chinese Materials Research Society.

http://dx.doi.org/10.1016/j.pnsc.2015.07.002

means leads to large energy consumption and is very costly. Increasing the vanadia concentration of VWTi is generally another way to improve the low-temperature performance [1,2]. Nevertheless, the excessive vanadium species not only generate large N_2O by-products but will also be volatilized during the catalyst operation, which is very hazardous to the environment and human health. Therefore, catalyst aiming to industrial application should both require superior low-temperature activity and exhibit environment friendly features. Therefore, it is necessary to take persistent efforts to make modifications of the current VWTi catalyst or to develop novel catalysts.

Some transition metal oxides such as PtO [6], NiO [7], FeO_x [8], CuO [9], MnO_x [8,9] and CeO_2 [7–11] have been proved effectively to improve the low-temperature activity of VWTi. The researchers attribute this promotion effect mainly to two aspects: the modification of the surface structure and the enhanced redox properties thus increasing $NO \rightarrow NO_2$ oxidation activity [6–11]. Among them, Ce modification appears to be more promising due to its better redox properties, acid–base properties and economic efficiency [12–15]. Nevertheless, it cannot be ignored that these catalysts commonly suffer from the severe deactivation induced by SO_2 permanently existing in the exhaust, especially at low temperatures. Generally, the deposition of ammonium sulfates on catalyst which are derived from the reaction of gaseous SO_3 with NH_3 could lead to pore plugging and blockage of the active sites [16–18]. The combination of metal sites with SO_x (SO_2/SO_3) may also result in concomitantly irreversible loss of active sites by forming metal sulfites/sulfates [13,18,19]. However, the deactivation and promotion effect on catalytic activity of CeO_2 in the presence of SO_2 were both reported in some literatures [13,20–22], which is quite different from other metal oxides, e.g. MnO_x and FeO_x. Therefore, it is imperative to investigate the influence of SO_2 on the NH_3-SCR activity of Ce-modified VWTi catalyst and understand the deactivation or promotion mechanism. This will further provide reference and guidance for improving the SO_2 durability over this type of catalyst.

The objective of this work is to prepare a Ce modified VWTi catalysts possessing comparable low-temperature activity with VWTi with high vanadia content. Furthermore, various characterizations were employed in order to explore the sulfur deactivation/promotion mechanism over this catalyst.

2. Experiment

2.1. Catalyst preparation

The WO_3–TiO_2, CeO_2–TiO_2 and CeO_2–WO_3–TiO_2 mixed oxides were prepared by a citric acid-aided sol–gel method. Corresponding amounts of $(NH_4)_{10} \cdot W_{12}O_{41} \cdot 5H_2O$, $Ce(NO_3)_3 \cdot 6H_2O$ and TiO_2 powders were used as the precursors. Citric acid was used as the complexing agent at twice the amount of the metal ions and polyethylene glycol was adopted at 10 wt% of the citric acid. Precursor salts or metal oxides, citric acid, polyethylene glycol, and deionized water were sufficiently mixed and magnetically stirred at 80 °C until a spongy gel was obtained. The obtained gel was dried at 110 °C overnight and submitted to calcination at 500 °C for 4 h. For comparison, the pure TiO_2 also underwent the same thermal treatment.

Table 1
Compositions and structural properties of the catalysts.

Catalyst	Nominal mass content (wt%)				S_{BET} ($m^2\ g^{-1}$)	TiO_2 crystallite size (nm)
	V_2O_5	CeO_2	WO_3	TiO_2		
V1Ti	1	0	0	99	89.4	24.5
V1WTi			10	89	85.8	26.2
V1CeTi		8	0	91	84.3	25.8
V1CeWTi		8	10	81	81.8	25.6
V3Ti	3	0	10	87	93.4	26.1

VTi, VWTi, VCeTi and VCeWTi catalysts were further synthesized by impregnating the as-received TiO_2, WO_3–TiO_2, CeO_2–TiO_2 and CeO_2–WO_3–TiO_2 oxides with NH_4VO_3 solution. After drying at 110 °C overnight, the impregnated powders were calcined at 500 °C for 3 h in a muffle. The synthesized catalysts are donated as V(x)Ti, V(x)WTi, V(x)CeTi and V(x)CeWTi with x representing the mass percentage of vanadia, as listed in Table 1.

2.2. Design and preparation of reference samples

In order to investigate the SO_2 deactivation mechanisms over different catalyst, a series of reference samples were prepared as follows, which were sieved to 40–60 mesh size for temperature-programmed decomposition (TPDC) or temperature-programmed surface reaction (TPSR) experiment.

2.2.1. Sulfated samples

The sulfated TiO_2, WO_3–TiO_2, CeO_2–TiO_2 and V_2O_5/TiO_2 samples were obtained by conducting treatment of TiO_2, WO_3–TiO_2 (10 wt% WO_3), CeO_2–TiO_2 (8 wt% CeO_2) and V_2O_5/TiO_2 (3 wt% V_2O_5) samples under the following conditions: 60 ppm SO_2, balanced with air at 250 °C for 3 h, which were donated as Ti–S, WTi–S, CeTi–S and VTi–S, respectively.

2.2.2. Samples mechanically mixed with $(NH_4)_2SO_4$

TiO_2, CeO_2 and V_2O_5 powder were sufficiently mixed with 10 wt% $(NH_4)_2SO_4$ powder (< 200 mesh size) in a ball mill (QM-3SP04, China) for 3 h, and the obtained samples were donated as R-NSM (R = Ti, Ce or V). CeO_2 and V_2O_5 powder were synthesized by calcinaton of $CeN_3O_9 \cdot 6H_2O$ and NH_4VO_3 at 500 °C for 4 h.

2.3. Activity measurement

The measurements of the steady-state activity were carried out in a fixed bed quartz reactor (inner diameter of 10 mm) with the effluent gases monitored by Thermo Nicolet 380 FTIR spectrometer. Samples of 200 mg sieved to 40–60 mesh were used for the evaluation. The reaction gas mixture consisted of 500 ppm NO,

500 pm NH_3, 5% O_2, and N_2 as balance. The total flow rate of the feeding gas was 500 ml min^{-1} and the gas hourly space velocity (GHSV) was approximately 150,000 h^{-1}. All pipes in the reactor system were heat-traced to 190 °C to prevent water condensation and ammonium nitrate deposition. The NO_x conversion and N_2 selectivity were calculated according to Eqs. (1) and (2), respectively.

$$NO_x \text{ conversion } (\%) = \left(1 - \frac{[NO]_{out} + [NO_2]_{out}}{[NO]_{in}}\right) \times 100 \quad (1)$$

$$N_2 \text{ selectivity } (\%) = \left(1 - \frac{[NO_2]_{out} + 2 \times [N_2O]_{out}}{[NH_3]_{in} + [NO]_{in} - [NH_3]_{out} - [NO]_{out}}\right) \times 100 \quad (2)$$

2.4. Catalyst characterization

X-ray diffraction (XRD) patterns of the catalysts were determined using a D/mas-RB diffractometer (Rigaku, Tokyo, Japan) at 40 kV and 120 mA equipped with Cu K_α radiation (λ=0.15418 nm). Powder XRD patterns were recorded at 0.02° intervals in the range of $20° \le 2\theta \le 80°$ with a scanning velocity of 4° min^{-1}. Identification of the crystalline phases was performed using JCPDS (Joint Committee on Powder Diffraction Standards) cards. The mean crystallite size of TiO_2 in the samples was calculated using the Scherrer's formula.

The specific surface areas of the samples were measured using the N_2 physisorption at −196 °C using the Brunner−Emmett−Teller (BET) method on an automatic surface analyzer (F-sorb 3400, China). Before the measurements, all samples were degassed at 220 °C for 2 h prior to the measurement.

Raman spectra were measured using a confocal Raman spectrometer (HORIBA Jobin Yvon, France) at room temperature and atmospheric pressure. The 633 nm line (5 mW at sample) of the laser was used for recording the Raman spectra with a resolution of 1 cm^{-1}. The Laser beam was focused onto an area 0.1 × 0.1 mm^2 in size of the sample surface.

H_2-TPR was performed on a Micromeritics Auto Chem II 2920 (USA) with H_2 signals monitored with an affiliated TCD detector. Sample of 50 mg in a U type quartz tube was preheated by a He flow at 300 °C for 30 min and then heated in a 10% H_2/Ar flow from 50 to 900 °C at a ramping rate of 10 °C min^{-1}.

A fixed-bed quartz reactor was used for NH_3-TPD test. After the NH_3-SCR reaction with the above gases feeding at a certain temperature for 3 h, 200 mg sample was flushed by N_2 at 30 °C for 1 h to remove physisorbed species. Then, the sample was ramped to 500 °C at a rate of 10 °C min^{-1} for NH_3 desorption. NH_3 storage capacity is obtained by calculating the total amount of desorbed NH_3 during the TPD process.

Temperature-programmed decomposition (TPDC) experiment was carried out in a tubular quartz reactor (inner diameter of 10 mm) with 10 °C min^{-1} ramp in a He flow of 500 ml min^{-1} up to 850 °C. The outlet gases were monitored during the decomposition process by a quadrupole mass spectrometer (Omnistar 200, Germany) through the detection of fragments at *m/e*=17 (NH_3+) and 64 (SO_2+). The *m/e* at 64 (SO_2+) are representative of both SO_2 and SO_3 in agreement with the literature [23], which are believed to originate from the decomposition of surface sulfites or sulfates species.

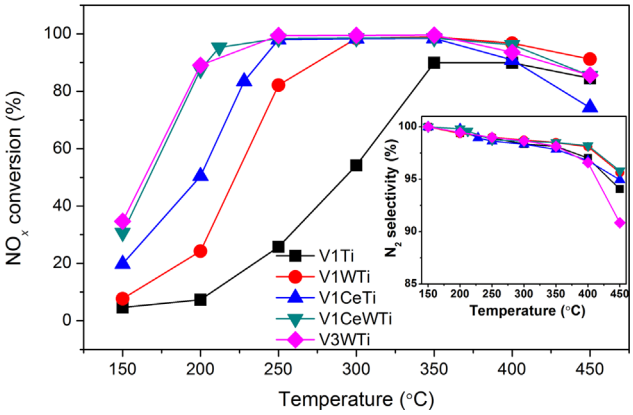

Fig. 1. NO_x conversions and N_2 selectivities of the catalysts. Reaction conditions: [NO]=[NH_3]=500 ppm, [O_2]=5% and N_2 as balance. GHSV=150,000 h^{-1}.

The SO_2 oxidation activity at certain temperature was measured in a fixed-bed quartz reactor under the following conditions: 200 mg sample (40–60 mesh), 180 ppm SO_2, 5% O_2, N_2 as balance, and GHSV=150,000 h^{-1}. Molar amount of SO_3 product was calculated by collecting $BaSO_4$ precipitates over 30 min after the reaction started. The SO_2 conversion was calculated by dividing the molar amount of SO_3 with total molar amount of inlet SO_2 during this 30 min experiment.

The reactivity of deposited $(NH_4)_2SO_4$ on the catalysts was measured using a temperature-programmed surface reaction (TPSR) with NO. Prior to the measurement, 200 mg catalyst was sufficiently mixed with 20 mg $(NH_4)_2SO_4$ powder using the above-mentioned method in Section 2.2.2. Subsequently, 20 mg $(NH_4)_2SO_4$ powder or the above samples were exposed to a stream consisting of 1000 ppm NO, 5% O_2, and N_2 as balance at a total flow rate of 500 ml min^{-1}. The temperature was ramped from 30 to 500 °C at a heating rate of 10 °C min^{-1} with the outlet NH_3 and NO concentrations real-timely monitored by the Thermo Nicolet 380 FTIR spectrometer.

3. Results

3.1. Catalytic performance

3.1.1. NH_3-SCR activity

The NH_3-SCR activities and N_2 selectivities of different catalysts are shown in Fig. 1. Among the catalysts prepared, V1CeWTi exhibits the widest operation temperature window (190–450 °C) at which the NO_x conversion and N_2 selectivity are higher than 80% and 95%, respectively. For four catalysts with 1 wt% V_2O_5 loading, the low-temperature (< 250 °C) activity is in the sequence of V1CeWTi > V1CeTi > V1WTi > V1Ti, indicating that the addition of ceria promotes the activities of both V1Ti and V1WTi catalysts. The N_2 selectivity of these samples at 450 °C follows the order of V1CeWTi > V1WTi > V1CeTi > V1Ti, indicating that both W and Ce species

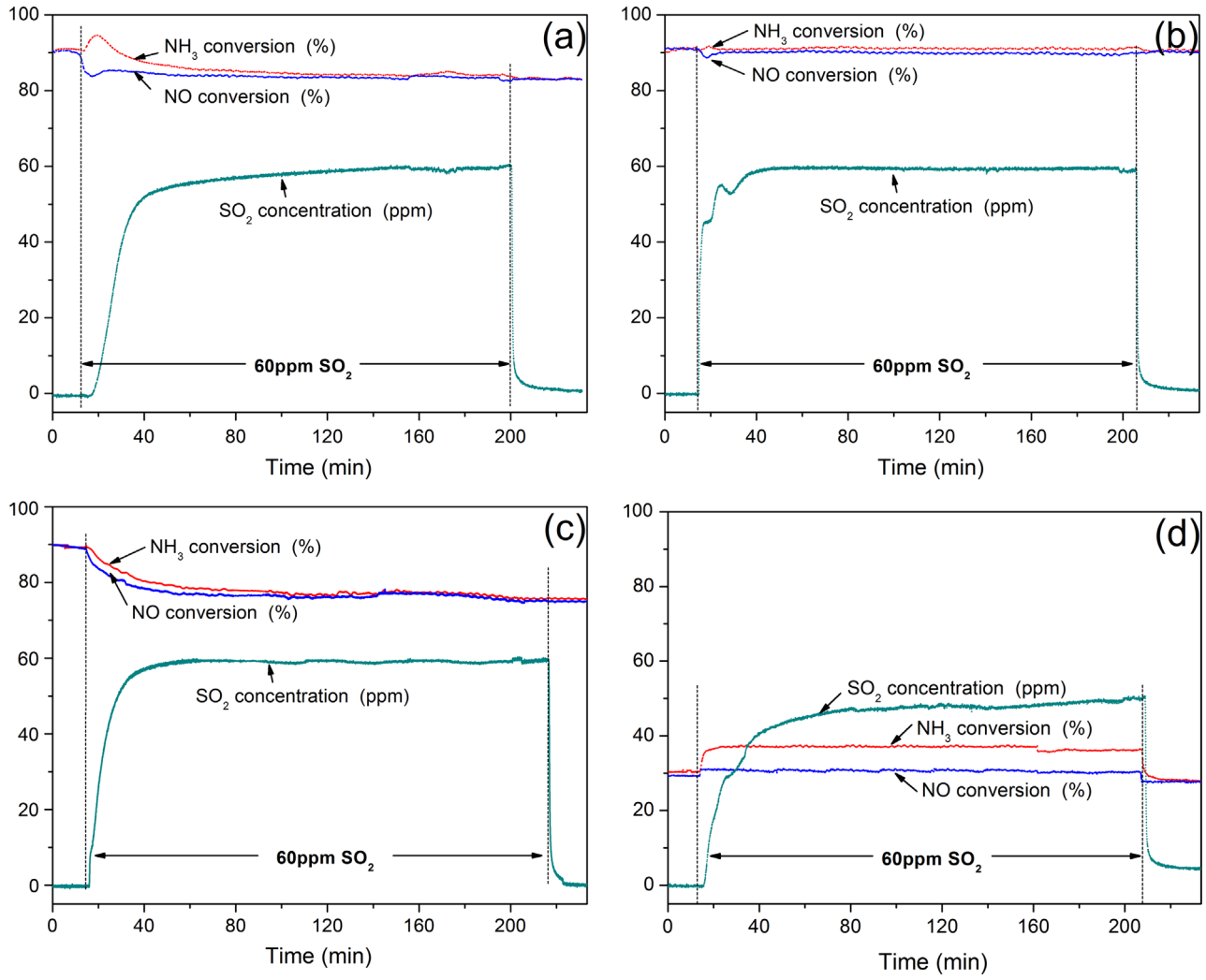

Fig. 2. The impacts of SO_2 addition and removal on the NH_3 and NO conversions over different catalysts. (a) V1WTi at 250 °C; (b) V3WTi at 190 °C; (c) V1CeWTi at 190 °C; and (d) V1Ti at 250 °C. Reaction conditions: [NO]=[NH_3]=500 ppm, [O_2]=5%, [SO_2]=60 ppm, and N_2 as balance. GHSV=150,000 h^{-1}.

could enhance N_2 selectivity at high temperatures. Although increasing the V_2O_5 loading to 3 wt% results in V3WTi catalyst with low-temperature activity similar to V1CeWTi, the excess usage of toxic vanadia is the main drawback of this catalyst.

3.1.2. *Influence of SO_2 on the SCR activity*

In order to investigate the effects of SO_2 on the catalytic performances of V1WTi, V3WTi, V1CeWTi and V1Ti, the transient responses of NH_3 and NO conversions to SO_2 introduction and removal were studied. The experiment on each catalyst was performed at the temperature when NO_x conversion reached 90%, at which the N_2 selectivity was always close to 100%. The NO conversion of V1WTi in Fig. 2a decreases slightly after introduction of SO_2 and is maintained at 85% at 250 °C, while that of V3WTi in Fig. 2b is almost unaffected by SO_2, indicating that increase of the vanadia content improves the resistance to SO_2. However, the NO conversion of V1CeWTi decreases slowly and finally stabilizes itself at 78% in the presence of SO_2 in Fig. 2c, indicating that Ce component is more sensitive to SO_2 poisoning and its addition decreases the sulfur resistance of V1WTi to a certain degree. After the removal of SO_2, the NO conversions of V1WTi and V1CeWTi could not recover to their initial levels, indicating that SO_2 leads to an irreversible deactivation of the catalyst. This is probably due to the deposition of ammonium sulfates and/or formation of metal sulfates.

In order to investigate the impact of W modification on the anti-sulfur performance of V1Ti catalyst, the transient response experiment of V1Ti to SO_2 was also performed at 250 °C. As shown in Fig. 2d, NH_3 conversion exceeds NO conversion by 7% in the presence of SO_2, implying that a portion of gaseous NH_3 contributes to the formation of ammonium sulfites/sulfates by reaction with SO_x (SO_2/SO_3). This is also verified by the fact that outlet SO_2 concentration is much lower than those over the other catalysts. It may be related to the low SCR activity over V1Ti catalyst which presents more chances for reaction between NH_3 and SO_x.

3.2. *Structural and redox properties*

3.2.1. *XRD*

Fig. 3 shows the XRD patterns of the catalysts. All the characteristic diffraction peaks are consistent with those of

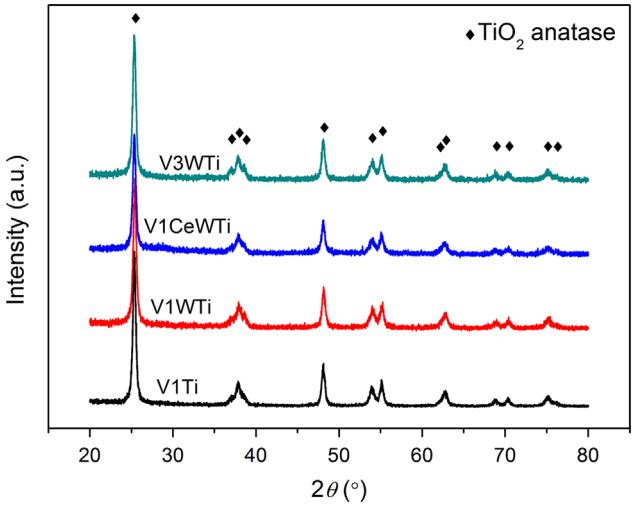

Fig. 3. XRD patterns of different catalysts.

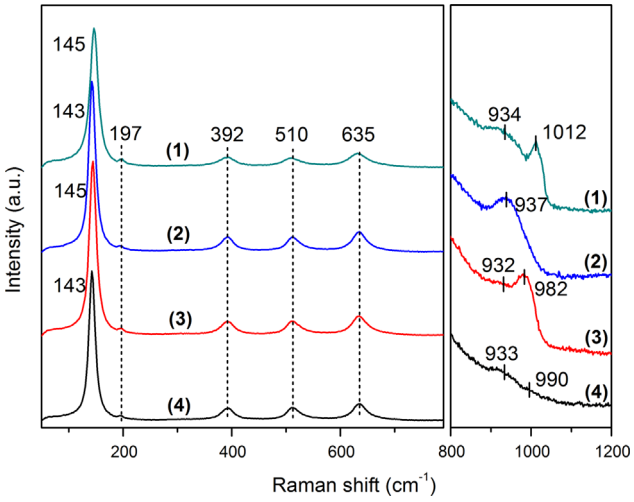

Fig. 4. Raman spectra of the catalysts. (1) V3WTi; (2) V1CeWTi; (3) V1WTi; (4) V1Ti.

anatase TiO_2. No crystalline phases related to V, W or Ce species are observed, suggesting that all these metal oxides exist in the form of highly dispersed surface species or amorphous compounds. Table 1 shows the structural properties of different samples. The BET surface areas of the samples are all larger than 80 $m^2\ g^{-1}$, indicating that all the catalysts were prepared with high specific surface area. There are no obvious changes in the crystallite sizes of TiO_2 in different samples.

3.2.2. Raman spectra

Raman spectra of different catalysts are presented in Fig. 4. The bands at 143–145, 197, 392, 510 and 635 cm^{-1} are detected on all the samples, which could be assigned to E_g, E_g, B_{1g}, A_{1g} and E_g modes of anatase TiO_2, respectively [24,25]. As for V1CeWTi, the F_{2g} mode of O–Ce–O vibrations which generally shows a band at 460 cm^{-1} [26] is not observed, indicating the absence of crystalline ceria on TiO_2 support, which is in consistent with the XRD result. Generally, the bands in the 800–1050 cm^{-1} range are characteristic of well dispersed VO_x or WO_x species on TiO_2. The bands at 933 and 990 cm^{-1} are assigned to V–O–V stretching vibrations of polymeric vanadate species and the V=O stretching vibration of isolated mono-vanadate species, respectively [12,26,27]. The bands at 982–1012 cm^{-1} in V1WTi and V3WTi appear in higher intensity than that in V1Ti, attributing to the presence of W=O vibration in surface WO_x species [25,28]. The broadening of the bands at 932–934 cm^{-1} to lower wavenumbers in these catalysts may be a result of the increased formation of V–O–V structures after WO_3 modification, in agreement with the literatures [25,29]. As for V1CeWTi catalyst, both the bands of V=O and W=O vibration are significantly weakened, and a new broad band appears at 937 cm^{-1}. This band is assigned to the vibrations of V–O–Ce and W–O–Ce structures, which is indicative of the strong interaction between surface CeO_x and VO_x/WO_x species [12,26,27]. It is also interesting to note that the typical VO_4^{3-} units possessing the most prominent band at 850 cm^{-1} are absent in this spectra, indicating that no $CeVO_4$ compound is formed in V1CeWTi catalyst [12,26,27].

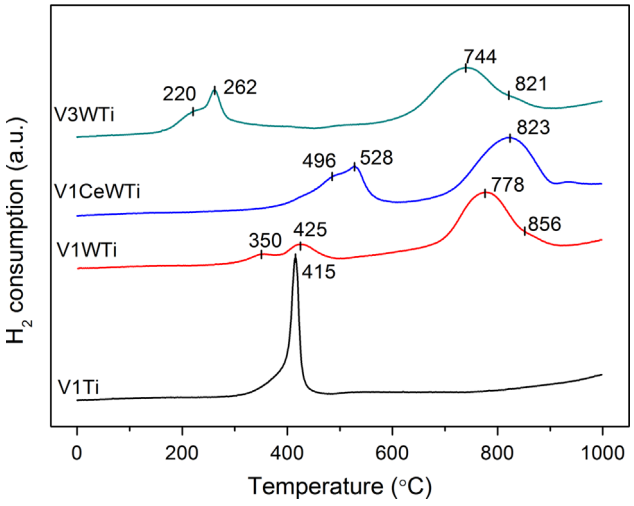

Fig. 5. H_2-TPR profiles of the catalysts.

3.2.3. H_2-TPR

Fig. 5 shows the H_2-TPR profiles to estimate the reducibility of different catalysts. According to the literatures [10,29], the distinct peak at 415 °C in V1Ti is attributed to the reduction of isolated VO_x species strongly bonded to TiO_2 support. After WO_3 addition, a shoulder peak at 350 °C appears, which is attributed to the reduction of polymeric VO_x species formed by connecting isolated VO_x species with bridging oxygen [8,10]. Clearly, the occupation of WO_x species on TiO_2 could induce the decreased interaction between VO_x and TiO_2 support and the polymerization of surface VO_x species. With the increase of the vanadia content, more facile reductions related to VO_x species on V3WTi occur in a lower temperature range 200–300 °C, which is due to the increasing polymerization degree

of VO_x species. The reduction peaks in the temperature range 650–900 °C for V(*x*)WTi catalysts are attributed to the reduction of surface WO_x species [29,30]. As for V1CeWTi, the peak at 496 °C arises from the interaction between CeO_2 and VO_x [12,31], while the peak at 528 °C is ascribed to the reduction of active oxygen from ceria [32,33]. The broad peak at 823 °C corresponds to the reduction of bulk CeO_2 and WO_x species [29,32]. In summary, the increase of the vanadia content and the introduction of WO_x can both enhance the reducibility of catalysts, and the addition of ceria also increases the amount of active oxygen available at the temperatures lower than 600 °C.

3.3. SO_2 poisoning mechanism

3.3.1. Surface species on the poisoned catalysts

In order to characterize ammonium sulfates and metal sulfates species formed on different catalysts during the NH_3-SCR reaction in a SO_2-containing atmosphere, the poisoned catalysts were heated up from room temperature to 850 °C in a He flow and the desorption curves of SO_x (SO_2+SO_3) are shown in Fig. 6. The amounts of NH_3 and SO_x desorption were calculated on a basis of this TPDC profiles and the results are summarized in Table 2.

The desorbed NH_3 can be attributed to two categories, i.e. the ammonia adsorbed on acid sites of catalysts and that from ammonium sulfates deposited on catalyst surface. NH_3-SCR reactions in the absence of SO_2 for 3 h were also conducted at the same temperature for each sample as analogous to the SO_2-added NH_3-SCR reaction. Thus, the desorbed NH_3 over each catalyst in the subsequent TPD (temperature-programmed desorption) process can be considered as the total amount of NH_3 bonded to acid sites, i.e. the NH_3 storage capacities at the reaction temperatures. Assuming that the original NH_3 storage capacity of each catalyst is invariant with SO_2 introduction, the amount of ammonium sulfates deposited on each sample can be calculated approximately based on the difference in amounts of desorbed NH_3 in the above two experiments. Further, the amount of metal sulfites/sulfates derived from reaction between metal sites and gaseous SO_x (SO_2/SO_3) can also be calculated by deducting the amount of ammonium sulfates from total SO_x amount. Accordingly, these data are also listed in Table 2.

As shown in Table 2, the modifications of both WO_3 and CeO_2 to V1Ti largely inhibit $(NH_4)_2SO_4$ deposition. The increase in the vanadia content could further results in less $(NH_4)_2SO_4$ species on catalysts. It is worth noting that the calculated amount of $(NH_4)_2SO_4$ species on different catalysts is in the sequence of V1Ti > V1WTi > V1CeWTi > V3WTi, correlating well with the gap areas between NO and NH_3 conversions as depicted in Fig. 2.

According to the literatures, ammonium sulfates decompose at 200–350 °C [19,34], while the decomposition temperatures of metal sulfites/sulfates are mediated at 350–850 °C depending on the metal ion-sulfates bonding strength [19]. It is shown that SO_x desorption on all catalysts in Fig. 6 occurs in the temperature range 350–850 °C, and only a small amount of SO_x is detected in the corresponding temperature range for NH_3 desorption (150–350 °C), indicating that outlet SO_x arises mainly from the decomposition of metal sulfites/sulfates on the catalysts except for V1Ti. This phenomenon is well consistent with the results in Table 2. It is clearly seen that the introduction of WO_3 can markedly inhibit the formation of metal sulfites/sulfates on VTi, and ceria component are more sensitive to SO_2 poisoning.

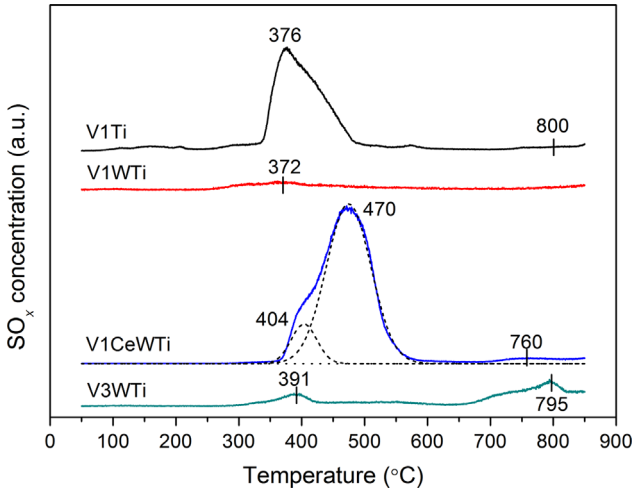

Fig. 6. TPDC profiles of metal sulfites/sulfates over the poisoned catalysts. Experimental conditions: 500 ml min^{-1} He, at a heating rate of 10 °C min^{-1}.

Table 2
Amounts of different surface species on the poisoned catalysts.

Sample	(μmol $g_{cat.}^{-1}$)				
	SO_x amount[a]	NH_3 amount[a]	NH_3 storage capacity[b]	Ammonium sulfates[c]	Metal sulfates[d]
V1Ti	1100.8	695.2	107.6	587.6	513.2
V1WTi	162.8	200.2	154.7	45.5	117.3
V1CeWTi	2041.0	243.4	226.7	16.7	2024.3
V3WTi	423.4	167.0	157.9	9.1	414.3

[a]Amounts estimated from the TPDC processes over the 200 mg samples after the NH_3-SCR reactions in the presence of SO_2 for 3 h.
[b]Amounts estimated from the TPD processes over the 200 mg samples pretreated with above experimental procedure in the absence of SO_2 for 3 h.
[c]Calculated as $(NH_4)_2SO_4$ species.
[d]Calculated as SO_4^{2-} anion group.

3.3.2. Decomposition of metal sulfites/sulfate species

In order to identify the surface sulfated species on each poisoned catalysts, a series of reference samples were treated in SO_2+O_2 and the sulfated samples were analyzed by TPDC experiment. In this process, SO_3 was generated as a product of SO_2 oxidation, and metal sulfites/sulfates were formed by the reactions between the SO_x (SO_2/SO_3) and surface metal sites. The temperatures for SO_x desorption give insights into the nature of typical metal sulfites/sulfates. Fig. 7 shows the TPDC profiles of the sulfated reference samples. A distinct desorption

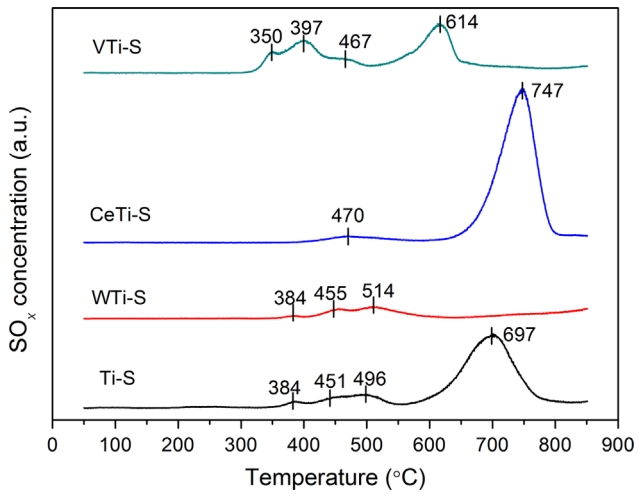

Fig. 7. TPDC profiles of metal sulfites/sulfates over the sulfated reference samples. Experimental conditions: 500 ml min^{-1} He, at a heating rate of 10 °C min^{-1}.

peak at 697 °C with three shoulders at 384, 451 and 496 °C are observed on Ti–S, which are derived from the successive decomposition of $Ti(SO_4)_2$ [35,36]. The first three desorption peaks appear on WTi–S at low temperatures (300–550 °C), whereas no signal of desorption peaks are observed at high temperatures, indicating only a small portion of surface Ti^{n+} sites are sulfated. This result reveals that the presence of WO_x species greatly prohibits the formation of stable $Ti(SO_4)_2$. The desorption peak at 470 °C corresponds to the decomposition of a small amount of $Ti(SO_4)_2$ on CeTi–S, while the peak at 747 °C is mainly attributed to the overlapping of decomposition of $CeOSO_4$ and $Ce_2(SO_4)_3$ [22,37–40]. This indicates that, SO_3 is more likely to react with ceria rather than titania. As for VTi–S, considering the SO_x desorption behavior is consistent with that on the Ti–S sample, the SO_x desorption peaks at 350, 397, 467 and 614 °C are mainly derived from the $Ti(SO_4)_2$ decomposition. Meanwhile, more metal sulfites/sulfates species are formed on VTi–S as indicated by the stronger intensity of SO_x desorption peaks at 300–550 °C, and the decomposition process shifts towards lower temperatures. All these suggest that VO_x species behave as active sites for the oxidation of SO_2 to SO_3 and leads to more severe sulfation of TiO_2.

Based on the above analysis, the assignment of metal sulfites/sulfates on different poisoned catalysts in Fig. 6 can be made. Accordingly, the main metal sulfites/sulfates species on V1Ti is $Ti(SO_4)_2$, and WO_x modification greatly suppresses the generation of $Ti(SO_4)_2$. Increasing the vanadia content is found to promote the sulfation of titania with stronger oxidation of SO_2. According to the literatures [22,37–39], $Ce(SO_3)_2$ or $Ce(S_2O_7)_2$ species decompose on V1CeWTi in a temperature range 400–500 °C, however, small portion of the stable $CeOSO_4$ and $Ce_2(SO_4)_3$ species still exist as indicated by the broad peak centered at 760 °C. These results indicate again that, ceria component can compete with titania in the reaction with SO_x, while WO_x species protects the titania support from being sulfated. These features are probably

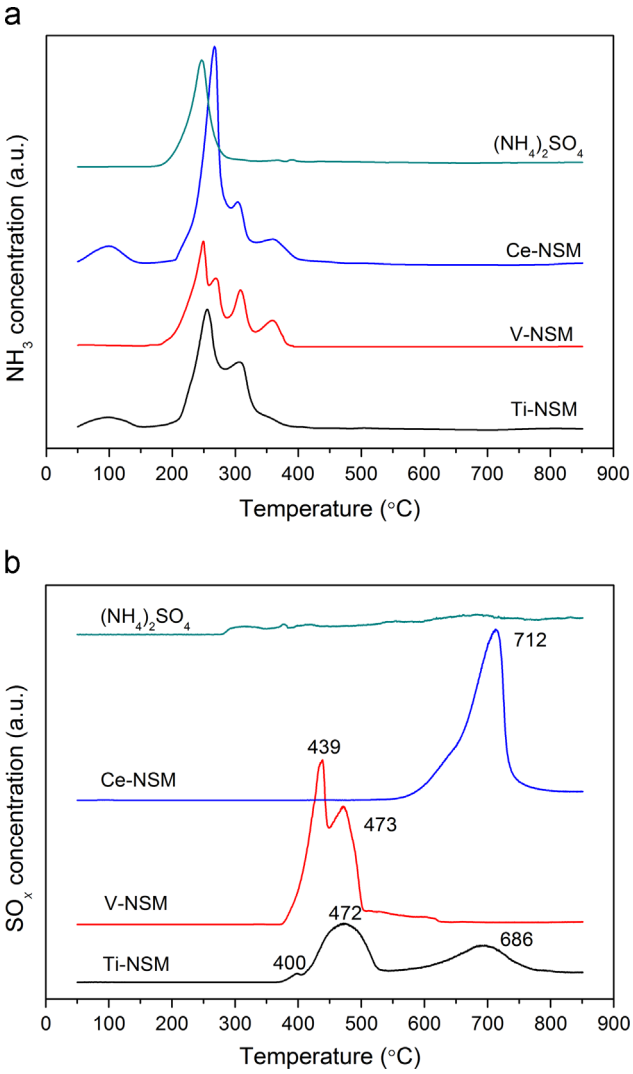

Fig. 8. The profiles of (a) NH_3 and (b) SO_x on different metal oxides mechanically mixed with $(NH_4)_2SO_4$ during the TPDC process.

related to the different acid–base properties of CeO_2, TiO_2 and WO_3.

3.3.3. Formation mechanism of metal sulfites/sulfate species

The metal oxides including V_2O_5, CeO_2 and TiO_2 mechanically mixed with $(NH_4)_2SO_4$ were also characterized by TPDC experiment and the results are shown in Fig. 8. NH_3 releases from pure $(NH_4)_2SO_4$ at around 200 °C, while the temperature at which SO_2 starts to release is approximately 270 °C. One important factor responsible for the different onset temperatures for NH_3 and SO_2 desorption is the successive decomposition process of ammonium sulfates, i.e., $(NH_4)_2SO_4 \rightarrow NH_4HSO_4 \rightarrow (NH_4)_2S_2O_7 \rightarrow NH_3 + SO_2$, in which ammonia releasing process is essentially ahead. NH_3 desorption peaks over all metal oxides are between 150–400 °C, which is consistent with the decomposition behavior of $(NH_4)_2SO_4$. However, the SO_2 desorption process occurs at higher temperatures (>400 °C) and shows substantial differences from

that on pure $(NH_4)_2SO_4$, indicating that these SO_4^{2-} groups are more strongly bonded to metal oxides. These results illustrate again that SO_4^{2-} groups in $(NH_4)_2SO_4$ could combine with the surface metal sites after desorption of NH_3 and leads to the formation of metal sulfites/sulfates within the NH_3-SCR temperature range (150–450 °C). In particular, the SO_2 peak centered at 712 °C on Ce-NSM is derived from the decomposition of cerium sulfates, which is in accordance with the result of CeTi–S in Fig. 7. Large amounts of unstable metal sulfates on V-NSM decompose at 439 and 473 °C, corresponding to the decomposition behaviors of $VOSO_4$ species [41]. By comparison of the TPD results of sulfated VTi shown in Fig. 7, the formation of $VOSO_4$ species cannot be excluded on VTi sample with only 1 wt% V_2O_5 loading.

3.3.4. SO_2 oxidation activity

In order to evaluate the SO_3 formation ability of different catalysts, the SO_2 oxidation experiments were performed and the results are shown in Fig. 9. The introduction of tungsten oxide improves the SO_2 conversion of V1Ti, and the further increase of the vanadia content also results in a significant increase in SO_2 oxidation activity. It has been reported that SO_2 oxidation activity over vanadium based catalysts is closely related to the redox property modulated by vanadium surface density [42]. With the introduction of WO_3 and increase of the vanadia content, the predominant structure of surface vanadia species changes from monomeric to polymeric form as indicated in Raman results, which contributes to better reducibility and higher SO_2 oxidation activity. The SO_2 oxidation activity of the Ce-modified catalyst is significantly higher than V1WTi. It is worth noting that, although the reduction peak temperatures of V1CeWTi are higher than those of V1WTi as shown in Fig. 5, the areas of the low-temperature reduction peaks are larger. According to the literatures [19,22,23], gas phase SO_2 is catalytically oxidized to SO_3 via the intermediate surface sulfates species (ads-SO_3 species). The introduction of ceria, which shows facile redox cycle between Ce^{3+} and Ce^{4+}, could be able to donate oxygen sites for SO_2 adsorption and promote the formation of cerium sulfates species [22], resulting in a significantly higher apparent SO_2 conversion as shown in Fig. 9.

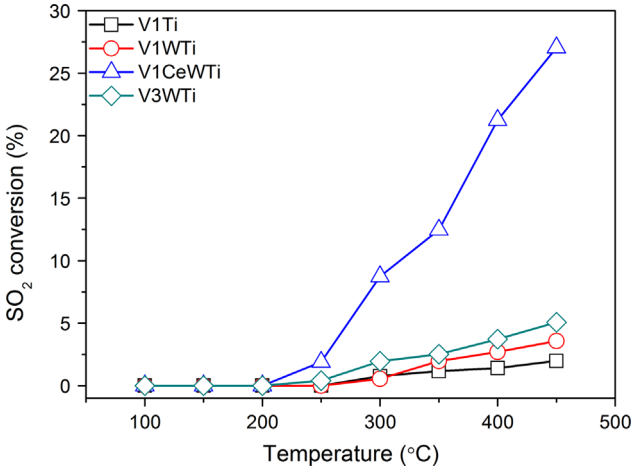

Fig. 9. The SO_2 oxidation activities of different catalysts. Reaction conditions: 180 ppm SO_2+5% O_2, N_2 as balance, GHSV=150,000 h^{-1}.

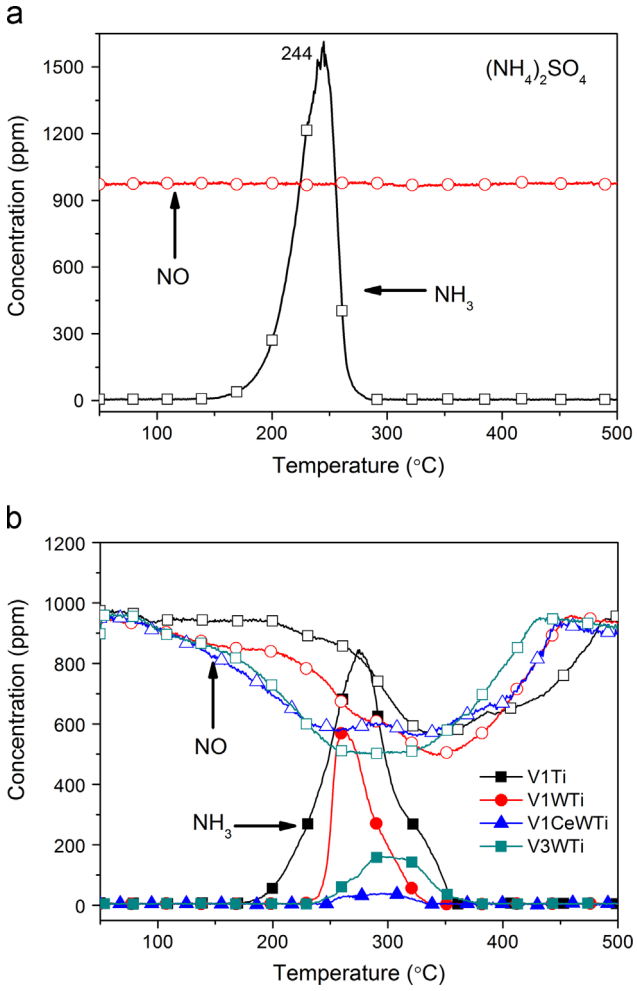

Fig. 10. TPSR profiles of NO with $(NH_4)_2SO_4$ (a) in pure state and (b) deposited on different catalysts. Reaction conditions: 1000 ppm NO+5% O_2 in N_2 (500 ml min^{-1}) at a heating rate of 10 °C min^{-1}.

3.3.5. Reactivity of the deposited $(NH_4)_2SO_4$

Fig. 10 shows the TPSR profiles of NO with $(NH_4)_2SO_4$ in the pure state or deposited on different catalysts. Pure $(NH_4)_2SO_4$ is impossible to participate in the reaction with NO, as indicated by the steady NO profile in the whole temperature range in Fig. 10a. The variations of NO concentration in Fig. 10b reflect different reactivity of $(NH_4)_2SO_4$ over different catalysts. This indicates that the active sites in catalyst play a crucial role in the catalytic decomposition of $(NH_4)_2SO_4$, which is in agreement with the literature [16]. Part of NH_4^+ species ($R-NH_4^+$) can react with NO over the catalysts, while the other part of NH_4^+ species ($D-NH_4^+$) desorbs in the form of gaseous NH_3. Therefore, it is predictable that the amount ratio of the $R-NH_4^+/(R-NH_4^+ + D-NH_4^+)$, which is defined as the reaction ratio, reflects the reactivity of $(NH_4)_2SO_4$ over the catalyst. The amounts of $R-NH_4^+$ and $D-NH_4^+$ were calculated by

Table 3
Data calculated from the TPSR results.

Sample	Desorbed NH_3 ($\mu mol\ g_{cat.}^{-1}$)	NH_3 involved in the reaction ($\mu mol\ g_{cat.}^{-1}$)	Reaction ratio (%)
V1Ti	509.4	574.4	53
V1WTi	208.9	709.4	77
V1CeWTi	17.8	717.2	98
V3WTi	95.6	750.6	89
$(NH_4)_2SO_4$	553.9	0	0

integrating the NO consumption and NH_3 desorption peaks, and the results are summarized in Table 3.

The initial consumption temperature for $(NH_4)_2SO_4$ over different catalysts follows the sequence of V1CeWTi ≈ V3WTi > V1WTi > V1Ti, which is consistent with the order of the low-temperature activity (< 250 °C) as shown in Fig. 1, implying that catalysts with high NH_3-SCR activity may be also beneficial to the reaction between the deposited $(NH_4)_2SO_4$ and NO.

4. Discussion

4.1. Active sites on V1CeWTi

It is known that the low-temperature SCR activity can be obviously enhanced on the Ce modified V_2O_5–WO_3/TiO_2 catalyst with a low vanadia loading. The V1CeWTi catalyst shows above 80% NO_x conversion and 95% N_2 selectivity from 190 to 450 °C, which exhibits comparable low-temperature (< 250 °C) activity with V3WTi. Considering the volatility of toxic vanadium species, the reduction in the vanadia content by ceria modification without loss of NH_3-SCR activity is beneficial to NO_x abatement industry. Therefore, V1CeWTi catalyst is an environmentally friendly and effective low-temperature NH_3-SCR catalyst.

The structure–activity relationship over the V_2O_5/TiO_2 catalyst has been revealed by several researchers [43], in which the activity is more related to V–O–V bridges rather than V=O groups. In Raman results, the addition of WO_3 into V1Ti promotes the polymerization of VO_x species by occupying the TiO_2 surface, and facilities the formation of V–O–V bridges as indicated by the broadening of the bands at 932–934 cm^{-1}. The increase of the vanadia content also promotes the polymerization of surface VO_x species. Strong interaction between CeO_2 and VO_x species is observed in the Raman spectrum and H_2-TPR profile. It has been reported that monomeric and polymeric VO_x would react with ceria to form $CeVO_4$ species in VO_x/CeO_2 supported catalyst [12,26]. However, no typical $CeVO_4$ species are found in Raman spectrum of V1CeWTi. Instead, V–O–Ce bridges are confirmed by the replacement of V=O group band by a new band at 937 cm^{-1} in Raman spectrum as well as the characteristic reduction peak at 496 °C in H_2-TPR profile. VO_x species anchored by V–O–Ce bridging mode are suggested to be more reactive than polymeric VO_x species in NH_3-SCR reaction [12,26,28], contributing to the high low-temperature activity over V1CeWTi catalyst.

4.2. SO_2 deactivation mechanism over V1CeWTi

It is shown in Fig. 2 and Table 2 that a significant $(NH_4)_2SO_4$ deposition occurs on V1Ti, while it is largely inhibited on V(x)WTi and V1CeWTi. Even though, the NO_x conversion in the presence of SO_2 for V1Ti catalysts is almost unaffected, indicating that the inhibition effect of $(NH_4)_2SO_4$ on active sites is limited. It is further discovered in Table 3 that an improved reactivity of deposited $(NH_4)_2SO_4$ with NO is obtained on V(x)WTi and V1CeWTi catalysts compared with V1Ti. According to the lower deposition degree and higher reactivity of $(NH_4)_2SO_4$ species, it is believed that the deactivation of V1CeWTi catalyst caused by SO_2 feeding should not arise from the impacts of $(NH_4)_2SO_4$ deposition on active sites. The very low ratio of $(NH_4)_2SO_4$ to total desorbed SO_x on V1CeWTi (0.8%) estimated from the data in Table 2 also implies this point.

However, $(NH_4)_2SO_4$, as an important intermediate species, always contributes to the formation of metal sulfites/sulfates under the NH_3-SCR conditions as shown in Fig. 8, leading to the irreversible loss of metal sites ($(NH_4)_2SO_4$ route). According to the literatures [19,22,23] and Fig. 7, the direct interaction between gaseous SO_3 and metal sites is an alternative formation route (SO_3 route) for metal sulfates. As listed in Table 2, the amount of metal sulfates formed via SO_3 route on different catalysts follows the sequence of V1CeWTi > V3WTi > V1WTi, indicating the introduction of ceria and increase in the vanadia content promote the formation of metal sulfites/sulfates. This correlates well with the sequence of $SO_2 \rightarrow SO_3$ oxidation activities over different catalysts. The proportion of metal sulfates formed via SO_3 route in total metal sulfates could be calculated by dividing the amount of metal sulfates by that of total SO_x, which turns to be 47%, 72%, 98% and 99% for V1Ti, V1WTi, V3WTi and V1CeWTi. This in turn illustrates the formation of metal sulfates via the other route ($(NH_4)_2SO_4$ route) is suppressed by WO_3 and CeO_2 modification and the increase of the vanadia content.

The almost unaffected catalytic activities on V1Ti and V1WTi as shown in Fig. 2 suggest V^{n+} sites on these catalysts are not tend to combine with SO_x to form sulfites/sulfates, which is also in agreement with the result that almost no $VOSO_4$ species is observed on VTi–S sample in Fig. 7. However, dramatically large amounts of these species are detected in Fig. 8b without TiO_2 support, which indicates that TiO_2 can behave as sacrificial agent to protect V^{n+} sites from being sulfated. The TiO_2 is reported to be only partially and reversibly sulfated on the catalyst surface due to the fast decomposition and formation cycle of Ti $(SO_4)_2$ in the NH_3-SCR reaction [1]. Both the results in Figs. 6 and 7 illustrate that the amount of the desorbed SO_x on V(x)WTi is far less than that on V1Ti, which indicates that the W modification helps to inhibit sulfation of TiO_2. Compared with TiO_2, Ce^{n+} sites are preferential to be sulfated by SO_2/SO_3 to form sulfates such as $CeOSO_4$ and $Ce_2(SO_4)_3$, which could disrupt the redox cycle between Ce^{3+} and Ce^{4+} and break the V–O–Ce bridges [8]. In this sense, the gradual decrease of NO conversion as shown in Fig. 2c is an indicative of deactivation of V1CeWTi by SO_2,

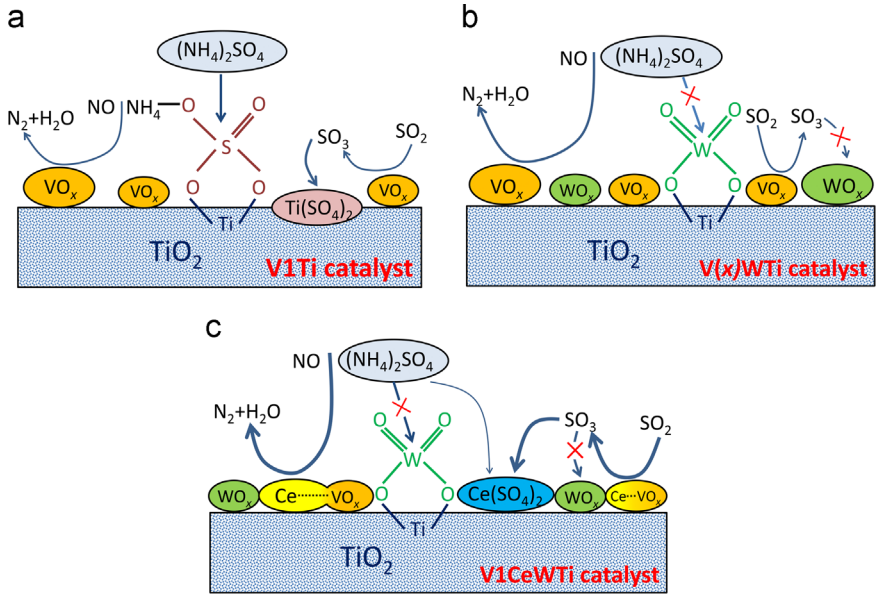

Scheme 1. The SO_2 deactivation mechanisms over different catalysts. (a) V1Ti; (b) V(*x*)WTi; (c) V1CeWTi.

where the remaining V^{n+} sites and probably some V–O–Ce bridges species still contribute to the high activity, as indicated by the steady NO conversion profile after 60 min.

Based on the above analysis, the schematic mechanisms for SO_2 deactivation over V1Ti, V(*x*)WTi and V1CeWTi catalysts are presented in Scheme 1. For V1Ti catalyst, the generation and deposition of $(NH_4)_2SO_2$ species on the catalyst surface are evident, which would further lead to the sulfation of Ti^{n+} sites. The direct reaction between TiO_2 support and SO_x is another route accounting for $Ti(SO_4)_2$ generation. Therefore, TiO_2 can act as a sacrificial agent to protect V^{n+} sites from sulfation. The polymeric WO_x species on V(*x*)WTi catalysts results in less formation and deposition of $(NH_4)_2SO_2$, which can be quickly consumed via reaction with NO on more reactive V^{n+} sites. The formation process of metal sulfates from the reaction of SO_4^{2-} groups and gaseous SO_3 with Ti^{n+} sites are both significantly blocked by WO_3 loading, leading to the superior resistance to SO_2 poisoning of V(*x*)WTi catalysts. Although the modification of ceria to V1WTi also inhibits $(NH_4)_2SO_2$ formation and deposition, the abundant oxygen sites in ceria are readily combinable with SO_2/SO_3, leading to severe sulfation of Ce^{n+} sites. This would further disrupt the redox cycle between Ce^{3+} and Ce^{4+} and deprive the synergistic effect between ceria and VO_x species.

5. Conclusions

The low-temperature catalytic activity of V_2O_5–WO_3/TiO_2 catalyst with 1 wt% vanadia loading was obviously enhanced by Ce modification in the NH_3-SCR of NO_x, and the V1Ce8W10Ti exhibited above 80% NO_x conversion and above 95% N_2 selectivity in a broad temperature range 190–450 °C. The synergistic effect between Ce and V contributed to the superior low-temperature activity by forming V–O–Ce bridges. SO_2 had little influence on the catalytic activities of VTi and VWTi catalysts, which is mainly due to the protection effect of TiO_2 support and WO_x species for active V^{n+} sites and low activity for SO_2 oxidation. The generation of SO_3 was significantly promoted on V1CeWTi catalyst. This, as well as the basic nature of ceria, caused the sulfation of ceria and accounted for the decrease in NO conversion from 90% to 78% in a SO_2-containing reaction atmosphere over this catalyst.

Acknowledgments

The authors would like to acknowledge the financial support from the National Science Foundation (No. 51202126) and the Key Laboratory of Solid Waste Reuse for Building Materials (SWR-2013-003).

References

[1] G. Busca, L. Lietti, G. Ramis, F. Berti, Appl. Catal. B: Environ. 18 (1998) 1–36.
[2] P. Forzatti, Appl. Catal. A Gen. 222 (2001) 221–236.
[3] K. Skalska, J.S. Miller, S. Ledakowicz, Sci. Total Environ. 408 (2010) 3976–3989.
[4] R.M. Heck, Catal. Today 53 (1999) 519–523.
[5] S. Roy, M.S. Hegde, G. Madras, Appl. Energy 86 (2009) 2283–2297.
[6] J.-H. Choi, J.-H. Kim, Y.-C. Bak, R. Amal, J. Scott, Korean J. Chem. Eng. 22 (2005) 844–851.
[7] Y. Xiao, T. Liang, P. Zhou, J. Mar. Eng. Technol. 11 (2012) 25–34.
[8] L. Chen, Junhua Li, M. Ge, J. Phys. Chem. C 113 (2009) 21177–21184.
[9] X. Tian, Y. Xiao, P. Zhou, W. Zhang, X. Luo, Mater. Res. Innov. 18 (2014) 202–206.
[10] X. Wang, A. Shi, Y. Duan, J. Wang, M. Shen, Catal. Sci. Technol. 2 (2012) 1386.
[11] M.A.L. Vargas, M. Casanova, A. Trovarelli, G. Busca, Appl. Catal. B Environ. 75 (2007) 303–311.
[12] Y. Peng, C. Wang, J. Li, Appl. Catal. B Environ. 144 (2014) 538–546.
[13] W. Xu, H. He, Y. Yu, J. Phys. Chem. C 113 (2009) 4426–4432.
[14] Y. Peng, J. Li, X. Huang, X. Li, W. Su, X. Sun, D. Wang, J. Hao, Environ. Sci. Technol. 48 (2014) 4515–4520.

[15] Z. Lian, F. Liu, H. He, Catal. Sci. Technol. 5 (2015) 389–396.
[16] Z. Zhu, H. Niu, Z. Liu, S. Liu, J. Catal. 195 (2000) 268–278.
[17] R. Jin, Y. Liu, Z. Wu, H. Wang, T. Gu, Catal. Today 153 (2010) 84–89.
[18] J. Yu, F. Guo, Y. Wang, J. Zhu, Y. Liu, F. Su, S. Gao, G. Xu, Appl. Catal. B Environ. 95 (2010) 160–168.
[19] S. BoXiong, L. Ting, Acta Phys-Chim. Sin. 26 (2010) 3009–3016.
[20] S. Yang, Y. Guo, H. Chang, L. Ma, Y. Peng, Z. Qu, N. Yan, C. Wang, J. Li, Appl. Catal. B Environ. 136–137 (2013) 19–28.
[21] T. Gu, Y. Liu, X. Weng, H. Wang, Z. Wu, Catal. Commun. 12 (2010) 310–313.
[22] R.M. Ferrizz, R.J. Gorte, J.M. Vohs, Catal. Lett. 82 (2002) 123–129.
[23] C. Orsenigo, L. Lietti, E. Tronconi, P. Forzatti, F. Bregani, Ind. Eng. Chem. Res. 37 (1998) 2350–2359.
[24] L. Chen, D. Weng, Z. Si, X. Wu, Prog. Nat. Sci.-Mater. 22 (2012) 265–272.
[25] C. Wang, S. Yang, H. Chang, Y. Peng, J. Li, Chem. Eng. J. 225 (2013) 520–527.
[26] Z. Wu, A.J. Rondinone, I.N. Ivanov, S.H. Overbury, J. Phys. Chem. C 115 (2011) 25368–25378.
[27] W. Daniell, A. Ponchel, S. Kuba, F. Anderle, T. Weingand, D. Gregory, H. Knözinger, Top. Catal. 20 (2002) 65–74.
[28] Y. Peng, K. Li, J. Li, Appl. Catal. B Environ. 140-141 (2013) 483–492.
[29] P.G.W.A. Kompio, A. Brückner, F. Hipler, G. Auer, E. Löffler, W. Grünert, J. Catal. 286 (2012) 237–247.
[30] Z. Ma, D. Weng, X. Wu, Z. Si, J. Environ. Sci.—China 24 (2012) 1305–1316.
[31] Z. Liu, S. Zhang, J. Li, J. Zhu, L. Ma, Appl. Catal. B Environ. 158–159 (2014) 11–19.
[32] Z. Ma, X. Wu, Z. Si, D. Weng, J. Ma, T. Xu, Appl. Catal. B Environ. 179 (2015) 380–394.
[33] Z. Ma, D. Weng, X. Wu, Z. Si, B. Wang, Catal. Commun. 27 (2012) 97–100.
[34] W.S. Kijlstra, M. Biervliet, E.K. Poels, A. Bliek, Appl. Catal. B Environ. 16 (1998) 327–337.
[35] K. Arata, M. Hino, N. Yamagata, Bull. Chem. Soc. Jpn. 63 (1990) 244–246.
[36] Y.G. Shul, H.J. Kim, S.J. Haam, H.S. Han, Res. Chem. Intermediat. 29 (2003) 849–859.
[37] X. Wu, H.-R. Lee, S. Liu, D. Weng, Ind. Eng. Chem. Res. 52 (2013) 716–721.
[38] X. Wu, H.-R. Lee, S. Liu, D. Weng, J. Rare Earth 30 (2012) 659–664.
[39] P.K. Cheekatamarla, A.M. Lane, J. Power Sources 154 (2006) 223–231.
[40] H. Chang, X. Chen, J. Li, L. Ma, C. Wang, C. Liu, J.W. Schwank, J. Hao, Environ. Sci. Technol. 47 (2013) 5294–5301.
[41] G. Paul, A. Choudhury, R. Nagarajan, C.N.R. Rao, Inorg. Chem. 42 (2003) 2004–2013.
[42] H. Kamata, H. Ohara, K. Takahashi, A. Yukimura, Y. Seo, Catal. Lett. 73 (2001) 79–83.
[43] I. Giakoumelou, C. Fountzoula, C. Kordulis, S. Boghosian, J. Catal. 239 (2006) 1–12.